

Many-body multipole indices revealed by real-space dynamical mean-field theory

Guoao Yang(杨国骜), Jianhui Zhou(周建辉), and Tao Qin(秦涛)
Citation: Chin. Phys. B, 2026, 35 (**6**): 060301. DOI: 10.1088/1674-1056/ae48c3
http://cpb.iphy.ac.cn; http://iopscience.iop.org/cpb

What follows is a list of articles you may be interested in

Superadiabatic stimulated Raman adiabatic passage between dressed states

Fangzhou Jin(金芳洲), Ao Wang(王奥), Yunlan Ji(季云兰), Hui Zhou(周辉), and Jianpei Geng(耿建培)
Chin. Phys. B, 2026, 35 (**1**): 010305. DOI: 10.1088/1674-1056/ade1c4

Observation of topology of non-Hermitian systems without chiral symmetry

Shuo Wang(王硕), Zhengjie Kang(康正杰), Hao Li(李浩), Jiaojiao Li(李姣姣), Yuanjie Zhang(张元杰), and Zhihuang Luo(罗智煌)
Chin. Phys. B, 2025, 34 (**11**): 110304. DOI: 10.1088/1674-1056/addcc1

Exceptional rings and non-Abelian topology in non-Hermitian high-spin systems

Peng-Zhen Sun(孙鹏震), Zhou-Tao Lei(雷周涛), and Yuan-Gang Deng(邓元刚)
Chin. Phys. B, 2025, 34 (**11**): 110303. DOI: 10.1088/1674-1056/addcbe

Antichiral edge states in a square lattice

Peng-Yu Guo(郭鹏宇), Wei Li(黎炜), Junhui Hu(胡君辉), and Hai-Xiao Wang(王海啸)
Chin. Phys. B, 2025, 34 (**10**): 100307. DOI: 10.1088/1674-1056/add90c

diabatic holonomic quantum computation in decoherence-free subspaces with two-body interaction

Xiaoyu Sun(孙晓雨), Lei Qiao(乔雷), and Peizi Zhao(赵培茊)
Chin. Phys. B, 2025, 34 (**9**): 090308. DOI: 10.1088/1674-1056/adeb5e

---

RAPID COMMUNICATION

Many-body multipole indices revealed by real-space dynamical mean-field theory

Guoao Yang(杨国骜)[1], Jianhui Zhou(周建辉)[2,†], and Tao Qin(秦涛)[1,‡]

[1] *School of Physics, Anhui University, Hefei* 230601, *China*

[2] *Anhui Key Laboratory of Low-energy Quantum Materials and Devices, High Magnetic Field Laboratory, HFIPS, Chinese Academy of Sciences, Hefei* 230031, *China*

(Received 26 December 2025; revised manuscript received 15 February 2026; accepted manuscript online 23 February 2026)

Multipole moments, fundamental characteristics of insulating materials, have garnered significant interest with the recent emergence of higher-order topological insulators. However, a practical method to explore them in correlated insulators is still lacking. Here, we introduce a systematic approach, which combines the general Green's function formula for multipoles with real-space dynamical mean-field theory, to calculate multipole moments in correlated materials. Our demonstration calculations for the correlated two-dimensional Benalcazar–Bernevig–Hughes model are consistent with symmetry analysis. This method opens a new avenue to study topological phase transitions in correlated multipole insulators and other crucial physical quantities closely related to multipole moments.

Keywords: higher-order topological insulator, multipoles, strongly correlated electron systems

PACS: 03.65.Vf, 42.25.Ja, 71.27.+a

DOI: 10.1088/1674-1056/ae48c3 **CSTR:** 32038.14.CPB.ae48c3

1. Introduction

The polarization, a fundamental property of insulators, is closely related to the integral of the Berry curvature in the parameter space and has been under intensive study for decades.[1–7] The emergence of topological insulators offers a new platform for the study of polarization, which works as a topological index for the topological phase transition. Meanwhile, a calculation formula for the polarization is proposed, and affords the possibility of exploring the polarization in the interacting case.[8] However, its implementation associated with a Lanczos algorithm makes the generalization to higher dimensions forbidden.[9,10] Therefore, a practical method to reveal the polarization in correlated insulators remains largely elusive.

The physics of polarization and its multipole generalization have become more active in the new field of higher-order topological insulators, which are characterized by quantized multipole indices.[11] The calculation of multipole moments in non-interacting systems, including crystalline[12] and non-crystalline systems,[13–15] has been carried out mainly using two methods. The first method is a direct generalization of Resta's formula[8] to multipole moments,[12,16,17] and the second is established by elaborating its relationship with the Wilson loop.[11,18] However, it is still difficult to incorporate interactions in these formalisms. Recently, there have been some attempts to take into account correlated effects for calculations of multipole moments, such as direct implementation of dynamical mean-field theory (DMFT),[19] quantum Monte Carlo combined with topological Hamiltonians,[20] and exact diagonalization with the infinite density matrix renormalization group.[21] Nevertheless, these methods exhibit three significant limitations: (1) they require direct access to the wave function of the many-body ground state, (2) they are unable to accommodate the inhomogeneity arising from the hopping term, and (3) their application to disordered systems presents substantial challenges.

Here, we propose a Green's function formalism in real space for the multipole indices, which can be perfectly fitted into the scheme of the real-space dynamical mean-field theory (R-DMFT)[22–24] with the advantages of considering inhomogeneity due to hopping and its implementation in a disordered system. We have carried out calculations of multipole indices for the one-dimensional (1D) Su–Schrieffer–Heeger (SSH) model and the correlated two-dimensional (2D) Benalcazar–Bernevig–Hughes (BBH) model with different spatial symmetries. The results are consistent with the symmetry analysis and shed light on the exploration of multipole indices of correlated insulators.

The rest of the manuscript has been organized as follows. In Section 2, we present our derivation details for the general formula of the multipoles, explain our protocol for combining them with R-DMFT, and point out potential further general-

†Corresponding author. E-mail: jhzhou@hmfl.ac.cn

‡Corresponding author. E-mail: taoqin@ahu.edu.cn

© 2026 Chinese Physical Society and IOP Publishing Ltd. All rights, including for text and data mining, AI training, and similar technologies, are reserved.

izations. In Section 3, we present the models explored in this work. In Section 4, we present demonstration results for the non-interacting 1D SSH model and the correlated 2D BBH model with different spatial symmetries. A summary and outlook are presented in Section 5.

2. Many-body multipole indices

We propose a Green's function formalism for the electrical polarization of a crystal, which is applicable to correlated systems,

$$P_x = \frac{1}{2\pi\mathcal{S}}\mathrm{Im}\left[\mathrm{Tr}\ln\left(\tilde{G}_x + I\right)\right] - P_{\mathrm{bg}}. \tag{1}$$

This is the central result of this work. Here $\tilde{G}_x = \alpha_x G$, $\alpha_x = \mathrm{diag}\{\mathrm{e}^{\frac{2\pi \mathrm{i} x_1}{L_x}} - 1, \ldots, \mathrm{e}^{\frac{2\pi \mathrm{i} x_N}{L_x}} - 1\}$, and G_x is a matrix of Green's functions with the i,jth element as $\langle c_i^\dagger c_j\rangle = \frac{1}{\beta}\sum_n G_{ij}(\mathrm{i}\omega_n)$, where $\omega_n = (2n+1)\pi/\beta$ is the Matsubara frequency, and $c_i^\dagger$ (c_j) is the creation (annihilation) operator on the lattice site i (j) in a supercell with sizes of L_x, L_xL_y, and $L_xL_yL_z$ for one-, two-, and three-dimensional cases, respectively. I is the identity matrix. $\mathcal{S}$ is dimension-dependent: $\mathcal{S} = 1$, L_y, L_yL_z for different dimensions, which is the area perpendicular to the x direction. $P_{\mathrm{bg}} = \frac{n_f}{\mathcal{S}}\sum_i \frac{x_i}{L_x}$ is the contribution from the background charge, with n_f the local density of electrical states. It can be combined with fixed boundary condition, periodic boundary condition, and a hybrid boundary condition. The generalization to include the spin flavor is straightforward.

We outline the crucial derivation steps for Eq. (1). Starting from the formula,[8,12] $P_x = \frac{1}{2\pi\mathcal{S}}\mathrm{Im}\left[\ln\langle\hat{U}_x\rangle\right] - P_{\mathrm{bg}}$, where $\langle\hat{U}_x\rangle = \langle GS|\hat{U}_x|GS\rangle = \langle GS|\,\mathrm{e}^{2\pi\mathrm{i}\sum_l \frac{x_l}{L_x}\hat{n}_l}|GS\rangle$, we have

$$\langle\hat{U}_x\rangle = \langle GS|\,\mathrm{e}^{2\pi\mathrm{i}\frac{x_1}{L_x}\hat{n}_1}\,\mathrm{e}^{2\pi\mathrm{i}\frac{x_2}{L_x}\hat{n}_2}\cdots\mathrm{e}^{2\pi\mathrm{i}\frac{x_N}{L_x}\hat{n}_N}|GS\rangle. \tag{2}$$

For the electron, we note the idempotency property of the electron number operator $\hat{n}_l^2 = \hat{n}_l$, which is a key observation here (see supplemental material for derivations of the spinful case). It follows that $\mathrm{e}^{2\pi\mathrm{i}\frac{x_l}{L_x}\hat{n}_l} = \sum_{m=0}^{\infty}\frac{1}{m!}\left(2\pi\mathrm{i}\frac{x_l}{L_x}\hat{n}_l\right)^m = 1 + \alpha_l\hat{n}_l$ with $\alpha_l = \mathrm{e}^{\frac{2\pi\mathrm{i}x_l}{L_x}} - 1$. Therefore, we come to

$$\begin{aligned}\langle\hat{U}_x\rangle &= \langle GS|\prod_{l=1}^{N}(1+\alpha_l\hat{n}_l)|GS\rangle,\\ &= 1 + \sum_{l=1}^{N}\alpha_l\langle\hat{n}_l\rangle + \sum_{1\le i<j\le N}\alpha_i\alpha_j\langle\hat{n}_i\hat{n}_j\rangle + \cdots,\end{aligned} \tag{3}$$

, where the last step is obtained by direct multiplication. We define a $N\times N$ matrix $\tilde{G}_x$, with $\left(\tilde{G}_x\right)_{ij} = \alpha_i\langle c_i^\dagger c_j\rangle$ ($i,j = 1,2,\ldots,N$). A second key observation[25] is that different orders of principal minors for $\det\tilde{G}_x$ coincide with different orders of terms for $\langle\hat{U}_x\rangle$ in Eq. (3) by Wick's theorem. As an example, we can see that the second-order principal minors of $\det\tilde{G}_x$ are $\alpha_i\alpha_j\begin{vmatrix}\langle\hat{n}_i\rangle & \langle c_i^\dagger c_j\rangle\\ \langle c_j^\dagger c_i\rangle & \langle\hat{n}_j\rangle\end{vmatrix}$, with $1\le i<j\le N$, which coincide with $\sum_{1\le i<j\le N}\alpha_i\alpha_j\langle\hat{n}_i\hat{n}_j\rangle$ in Eq. (3) by applying Wick's theorem to the latter form. Furthermore, assuming the eigenvalues of $\tilde{G}_x$ are λ_i ($i = 1,2,\ldots,N$), we have an identity for $\langle\hat{U}_x\rangle$ with eigenvalues as[26]

$$\langle\hat{U}_x\rangle = 1 + \sum_{i=1}^{N}\lambda_i + \sum_{1\le i<j\le N}\lambda_i\lambda_j + \cdots. \tag{4}$$

Compared with the characteristic polynomials $\det\left(\tilde{G}_x - \lambda I\right) = (-\lambda)^N + (-\lambda)^{N-1}\sum_{i=1}^{N}\lambda_i + (-\lambda)^{N-2}\cdot\sum_{1\le i<j\le N}\lambda_i\lambda_j + \cdots$, and setting $\lambda = -1$, we find

$$\langle\hat{U}_x\rangle = \det\left(\tilde{G}_x + I\right). \tag{5}$$

. Therefore, we finally have the polarization in the formalism of Green's functions,

$$P_x = \frac{1}{2\pi\mathcal{S}}\mathrm{Im}\left[\ln\det\left(\tilde{G}_x + I\right)\right] - P_{\mathrm{bg}}. \tag{6}$$

With the identity $\mathrm{Tr}\ln A = \ln\det A$, we have obtained Eq. (1). We have a remark here on the numerical implementation. As is known, polarization is an intensive quantity. In practical calculations, one cannot adopt Eq. (6), of which the first term tends to go to zero in the thermodynamic limit in more than one-dimensional space,[27] because numerically the imaginary part of the logarithm function lies in the interval $[-\pi,\pi)$; the complex logarithm is multi-valued. If one computes $\ln\det(\cdots)$ in Eq. (6) as a single complex number, the result is implicitly forced onto one particular branch, and the resulting intensive quantity $\frac{1}{\mathcal{S}}\ln\det(\cdots)$ would vanish in the thermodynamic limit $\mathcal{S}\to\infty$. In contrast, the quantity $\frac{1}{\mathcal{S}}\mathrm{Tr}\ln(\cdots)$ in Eq. (1) scales with the size of matrix $\tilde{G}$, similar to the 1D case. Therefore, one can obtain a proper value.

Similarly, we can write down the formula for the quadrupole moment in a crystal,

$$Q_{xy} = \frac{1}{2\pi\mathcal{L}}\mathrm{Im}\left[\mathrm{Tr}\ln\left(\tilde{G}_{xy} + I\right)\right] - Q_{\mathrm{bg}}. \tag{7}$$

Here $\tilde{G}_{xy} = \alpha_{xy}G$, and $\alpha_{xy} = \mathrm{diag}\{\mathrm{e}^{\frac{2\pi\mathrm{i}x_1y_1}{L_xL_y}} - 1, \ldots, \mathrm{e}^{\frac{2\pi\mathrm{i}x_Ny_N}{L_xL_y}} - 1\}$. $\mathcal{L} = 1$, L_z for two- and three-dimensional cases, which is the length perpendicular to the $x-y$ plane. $Q_{\mathrm{bg}} = \frac{n_f}{\mathcal{L}}\sum_i\frac{x_iy_i}{L_xL_y}$. A generalization to the case of the octupole moment is straightforward.

The key issue in the calculations in Eqs. (1) and (7) is to obtain the matrix of the Green's function G, and we are interested in correlated systems described by the fermionic Hubbard model. It is necessary to obtain G of a correlated lattice model to calculate many-body multipole moments. Real-space dynamical mean-field theory (R-DMFT)[19,22–24] is perfectly suitable for this purpose. In this scheme, a strongly correlated system on a lattice is mapped onto a group of impurities on lattice sites with the same spatial symmetry, along with hopping between different sites. In this way, both the onsite interactions and the inhomogeneity due to hopping are taken into

account. One then solves the DMFT problem on all sites until it is fully converged. Therefore, the interaction effects are taken into account at the DMFT level. Once the R-DMFT loop is converged, we then adopt Eqs. (1) and (7) to compute multipole indices. The flow chart for the whole computation process is shown in Fig. 1, which can be mostly divided into two parts: (1) the R-DMFT part and (2) the computation of many-body multipole indices. We comment on the efficiency of this algorithm. The most time-consuming part would be the R-DMFT routines, which can be accelerated with parallel implementation and optimized by spatial symmetry considerations. With a convergent Green's function, the calculations of multipole indices are quite efficient.

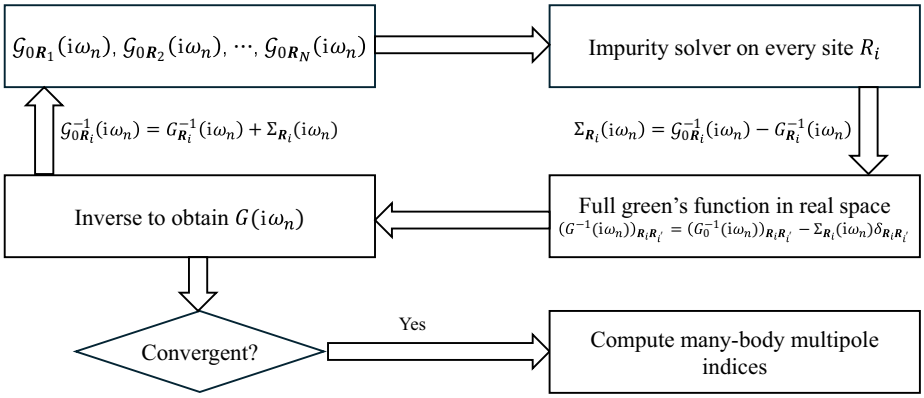


Fig. 1. Flowchart to compute the many-body multipole indices with the real-space dynamical mean-field theory (R-DMFT) and the Green's function formula for the multipole indices in the real-space. The R-DMFT is featured in Anderson impurities on every lattice site, self-consistently dealt with impurity solver to obtain $\Sigma_{\boldsymbol{R}_i}(\mathrm{i}\omega_n)$ on site $\boldsymbol{R}_i$, and meanwhile, the hopping taken into account by $\left(G_0^{-1}(\mathrm{i}\omega_n)\right)_{\boldsymbol{R}_i\boldsymbol{R}_{i'}}$. The computation of the multipole indices takes place when the R-DMFT loop is convergent with the Weiss field $\mathcal{G}_{0\boldsymbol{R}_i}(\mathrm{i}\omega_n)$.

The computational protocol shown in Fig. 1 is implemented as follows:

(1) Initialize the Weiss fields $\mathcal{G}_{0\boldsymbol{R}_i}(\mathrm{i}\omega_n)$ on all real-space sites $\boldsymbol{R}_i$.

(2) Solve the impurity problem on each site $\boldsymbol{R}_i$ using an impurity solver to obtain the local impurity Green's function $G_{\boldsymbol{R}_i}(\mathrm{i}\omega_n) = [G(\boldsymbol{R}_i, \boldsymbol{R}_j, \mathrm{i}\omega_n)]_{i=j}$, and update the local self-energy via $\Sigma_{\boldsymbol{R}_i}(\mathrm{i}\omega_n) = \mathcal{G}^{-1}_{0\boldsymbol{R}_i}(\mathrm{i}\omega_n) - G^{-1}_{\boldsymbol{R}_i}(\mathrm{i}\omega_n)$.

(3) Construct the full lattice Green's function in real space by assembling the matrix Dyson equation $G^{-1}(\mathrm{i}\omega_n) = \mathcal{G}_0^{-1}(\mathrm{i}\omega_n) - \Sigma(\mathrm{i}\omega_n)$, and invert the matrix to obtain $G(\mathrm{i}\omega_n) = [G(\boldsymbol{R}_i, \boldsymbol{R}_j, \mathrm{i}\omega_n)]$.

(4) Update the Weiss field using the DMFT self-consistency condition $\mathcal{G}^{-1}_{0\boldsymbol{R}_i}(\mathrm{i}\omega_n) = G^{-1}_{\boldsymbol{R}_i}(\mathrm{i}\omega_n) + \Sigma_{\boldsymbol{R}_i}(\mathrm{i}\omega_n)$, and iterate steps (2)–(4) until convergence by calculating the absolute value of the difference of $\mathcal{G}_{0\boldsymbol{R}_i}(\mathrm{i}\omega_n)$ between successive steps.

(5) After the R-DMFT loop converges, compute the many-body polarization/quadrupole indices using Eqs. (1) and (7).

In the R-DMFT iterations, self-consistency is monitored by the changes in all the local Weiss Green's functions between successive iterations. Concretely, for the Weiss Green's function in the k-th and $(k+1)$-th iterations, we require $\sum_{n,i}\left|\mathcal{G}^{(k+1)}_{0\boldsymbol{R}_i}(\mathrm{i}\omega_n) - \mathcal{G}^{(k)}_{0\boldsymbol{R}_i}(\mathrm{i}\omega_n)\right| \leq 10^{-5}$, where the value of the error can be slightly adjusted for different cases. In the second-to-last paragraph of Section 2, we pointed out that the numerically difficult part was to invert $G^{-1}(\mathrm{i}\omega_n)$ to obtain the full lattice Green's function, scaling with N^3, with N being the matrix size. Therefore, for the case of systems with large sizes, a parallel implementation of matrix inversion is necessary.

We comment on the limitations of our method. On one hand, the numerical constraints on our calculations arise from inverting $G^{-1}(\mathrm{i}\omega_n)$ to obtain $G(\mathrm{i}\omega_n)$, where the dimension of $G^{-1}(\mathrm{i}\omega_n)$ is $N \times N$, with N representing the number of lattice sizes. Mathematically, it is known that the computational complexity of matrix inversion is $\mathcal{O}\left(N^3\right)$, constituting the most time-consuming part of our calculations. On the other hand, when non-local effects are important, or inter-site Coulomb interactions are significant, one must take the self-energy among different sites into account, which is beyond the reach of our DMFT implementation.

To sum up, we have achieved two significant advancements. (1) We have a formula in the formalism of real-space Green's functions for the multipole indices, which can be implemented without requirement of wave-function of many-body ground state and is ready to be combined with the DMFT method, the real space formalism applicable to systems without translational symmetry, and one can further introduce disorder to lattices to explore the rich physics of disorder effects, quasi-crystal lattice,[28] amorphous lattices,[29,30] and so on. (2) With the multipole indices as a bridge, one can certainly study the localization length of the electron,[10] the polarization fluctuation,[31] and the quantum geometric tensor[32] in the correlated lattices.

3. The models

In this section, we present the models that we are going to investigate: the non-interacting one-dimensional Su–Schrieffer-Heeger model with staggered potentials in Eq. (8) and the interacting BBH model with staggered potentials in Eq. (9). We use the former model as a benchmark for our general formula in Eq. (1), and focus on the latter as a demonstration of our R-DMFT protocol.

The Hamiltonian of a one-dimensional SSH model with staggered potentials (see Fig. 2(a)) is

$$H_{\rm SSH} = \sum_{\boldsymbol{R}} \left(\gamma_x c^\dagger_{\boldsymbol{R}1} c_{\boldsymbol{R}2} + \lambda_x c^\dagger_{\boldsymbol{R}2} c_{\boldsymbol{R}+\hat{x}1} + \text{h.c.}\right) + \sum_{\boldsymbol{R}} \left(\Delta_x c^\dagger_{\boldsymbol{R}1} c_{\boldsymbol{R}1} - \Delta_x c^\dagger_{\boldsymbol{R}2} c_{\boldsymbol{R}2}\right). \tag{8}$$

For the SSH model, its Hamiltonian exhibits mirror symmetry $U_M = \sigma_1$ with respect to the unit cell. The onsite staggered potential Δ_x breaks the mirror symmetry of the system. The interacting BBH model[11,18] on a two-dimensional lattice with Hubbard interaction and staggered potentials (in Fig. 2(b)) reads

$$H^{\rm Hubbard}_{\rm BBH} = H_0 + H_{\rm stagger} + U\sum_{\boldsymbol{R}\gamma} n_{\boldsymbol{R}\gamma\uparrow} n_{\boldsymbol{R}\gamma\downarrow}, \tag{9}$$

where

$$\begin{aligned} H_0 = \sum_{\boldsymbol{R}\sigma} \Big[& \gamma_x \left(c^\dagger_{\boldsymbol{R}1\sigma} c_{\boldsymbol{R}3\sigma} + c^\dagger_{\boldsymbol{R}2\sigma} c_{\boldsymbol{R}4\sigma}\right) \\ & + \gamma_y \left(c^\dagger_{\boldsymbol{R}1\sigma} c_{\boldsymbol{R}4\sigma} - c^\dagger_{\boldsymbol{R}2\sigma} c_{\boldsymbol{R}3\sigma}\right) \\ & + \lambda_x \left(c^\dagger_{\boldsymbol{R}1\sigma} c_{\boldsymbol{R}+\hat{x}3\sigma} + c^\dagger_{\boldsymbol{R}4\sigma} c_{\boldsymbol{R}+\hat{x}2\sigma}\right) \\ & + \lambda_y \left(c^\dagger_{\boldsymbol{R}1\sigma} c_{\boldsymbol{R}+\hat{y}4\sigma} - c^\dagger_{\boldsymbol{R}3\sigma} c_{\boldsymbol{R}+\hat{y}2\sigma}\right)\Big] + \text{h.c.}, \end{aligned} \tag{10}$$

and $H_{\rm stagger}$ is the onsite staggered potential. The non-interacting part H_0 is a standard toy model of the higher-order topological insulator. In general, spatial symmetries are closely related to the quantization of the polarization and quadrupole moments.[11,18] By the term $H_{\rm stagger}$ we can tune the spatial symmetry and explore the correlation effects by introducing the Hubbard interaction term. We are mainly interested in two cases with different spatial symmetries as follows: case (i) $H_{\rm stagger} = \Delta_{xy}\sum_{\boldsymbol{R}\sigma}(n_{\boldsymbol{R}1\sigma} + n_{\boldsymbol{R}2\sigma} - n_{\boldsymbol{R}3\sigma} - n_{\boldsymbol{R}4\sigma})$, which preserves the spatial inversion symmetry, and case (ii) $H_{\rm stagger} = \Delta_x \sum_{\boldsymbol{R}\sigma}(n_{\boldsymbol{R}1\sigma} - n_{\boldsymbol{R}2\sigma} - n_{\boldsymbol{R}3\sigma} + n_{\boldsymbol{R}4\sigma})$ or $H_{\rm stagger} = \Delta_y \sum_{\boldsymbol{R}\sigma}(n_{\boldsymbol{R}1\sigma} - n_{\boldsymbol{R}2\sigma} + n_{\boldsymbol{R}3\sigma} - n_{\boldsymbol{R}4\sigma})$, which respect mirror symmetry along the y-direction (or the x-direction).

The system has the following symmetries: mirror symmetry: $U_{M_x} = \tau_1 \otimes \sigma_3$, $U_{M_y} = \tau_1 \otimes \sigma_1$, and inversion $\mathcal{I}$, and rotation C_2: $U_{\mathcal{I}} = U_{C_2} = U_{M_x} U_{M_y} = \mathrm{i}\tau_0 \otimes \tau_2$. The on-site staggered potential Δ_x (Δ_y) breaks mirror symmetry along the y-direction (x-direction), and the on-site staggered potential Δ_{xy} breaks both mirror symmetries along the x and y directions, but preserves the spatial inversion symmetry.

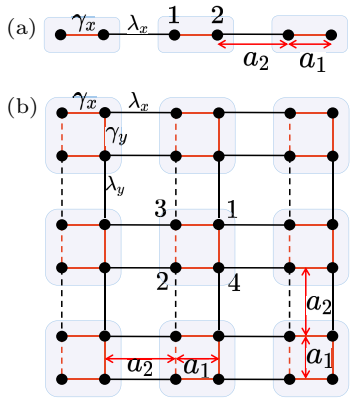


Fig. 2. The schematics of (a) 1D SSH model and (b) 2D BBH model, where dashed lines have a negative sign. a_1 and a_2 are lattice distances. We set $a_1 = a_2$ in our calculations.

4. Results and discussion

In this section, we first present the models that we are going to investigate. We start with a benchmark calculation for the non-interacting SSH model. Then, we present our main results for quadrupole moments in the interacting BBH model.

First, as a benchmark of Eq. (1), we perform a calculation of the polarization in the one-dimensional SSH model without interactions. As shown in Fig. 3, there are quantized polarization components P_x and sharp topological phase transitions in the non-interacting case. For the 1D SSH model, the onsite staggered potential Δ_x breaks the quantized polarization by removing the mirror symmetry about the x axis. This result is consistent with the common understanding of the 1D SSH model in Refs. [12,33], both of which developed real-space formalisms to calculate topological invariants of the 1D SSH model. Because the DMFT approximation is not applicable to 1D systems, we do not turn on interactions for the 1D case.

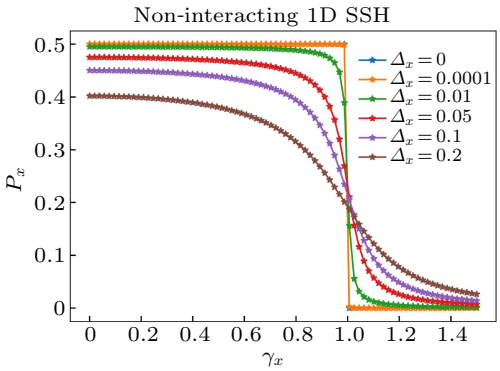


Fig. 3. The polarization in 1D non-interacting SSH model with $N_x = 100$.

Secondly, as a demonstration of our general protocol for calculating the quadrupole indices in correlated insulators, we present results for the quadrupole moments of the interacting 2D BBH model when the onsite staggered potential is nonzero, which provides a way to tune the spatial symmetry. For the R-DMFT calculations, an impurity solver based on iterative perturbation theory[19] is adopted. We choose periodic boundary conditions for the lattices, work at half-filling with $n_f = \frac{1}{2}$, and

focus on the paramagnetic phase. As a side remark, we point out that all multipole moment data are presented modulo 1.

The quantization of the quadrupole moment requires the system to have mirror symmetry about both x and y axes. For non-interacting systems, all three types of onsite staggered potentials Δ_x, Δ_y, and Δ_{xy} will destroy the quantized quadrupole moment by breaking the mirror symmetry of the system (see Fig. S1 in supplemental material for details). In the following, we focus on case (i) of the staggered potential Δ_{xy}.

We then present results of the 2D correlated BBH model calculated with the protocol in Fig. 1 (see Ref. [12] and Fig. S1 in supplemental material for the non-interacting case). As shown in Figs. 4(a) and 4(b) for the weakly interacting case, the quadrupole moment Q_{xy} stays quantized as long as the mirror symmetry conditions for quantization are preserved. In Fig. 4(c), the quantization fades away when the onsite staggered potential Δ_{xy} is turned on. It shows that the mirror symmetry is a dominant factor for the quantization of the quadrupole moment in the paramagnetic phase. We have similar observations for the strongly interacting case in Figs. 4(d)–4(f). There are differences in two respects. (1) The phase transition point deviates from $\gamma_x = \gamma_y = 1$ for the strongly interacting case. This deviation can be attributed to finite-size effects; the phase transition point shifts by about $\gamma_x = \gamma_y = 1$ and decreases with increasing system size (see Fig. S2 in supplemental material for details). (2) The transition due to γ_x jumps from 0.5 to 1, which is in fact $1 - 0^+$ with 0^+ being a positive tiny quantity, and is equivalent to 0^+ in the modulo calculation. Therefore, we show that even in the correlated regime, the quantization of the quadrupole moment is still determined by the spatial symmetry of the system.

In Fig. 5, we show the spectral functions for four different sites in one unit cell. The gaps due to interactions, together with emergent side-bands in Figs. 5(b) and 5(c) for very strong interactions, clearly indicate that the system is driven into the Mott insulator phase when the interaction U is large enough. Together with Fig. 4, we conclude that when spatial symmetries are preserved, even strong correlation does not preclude quantized quadrupole moments.

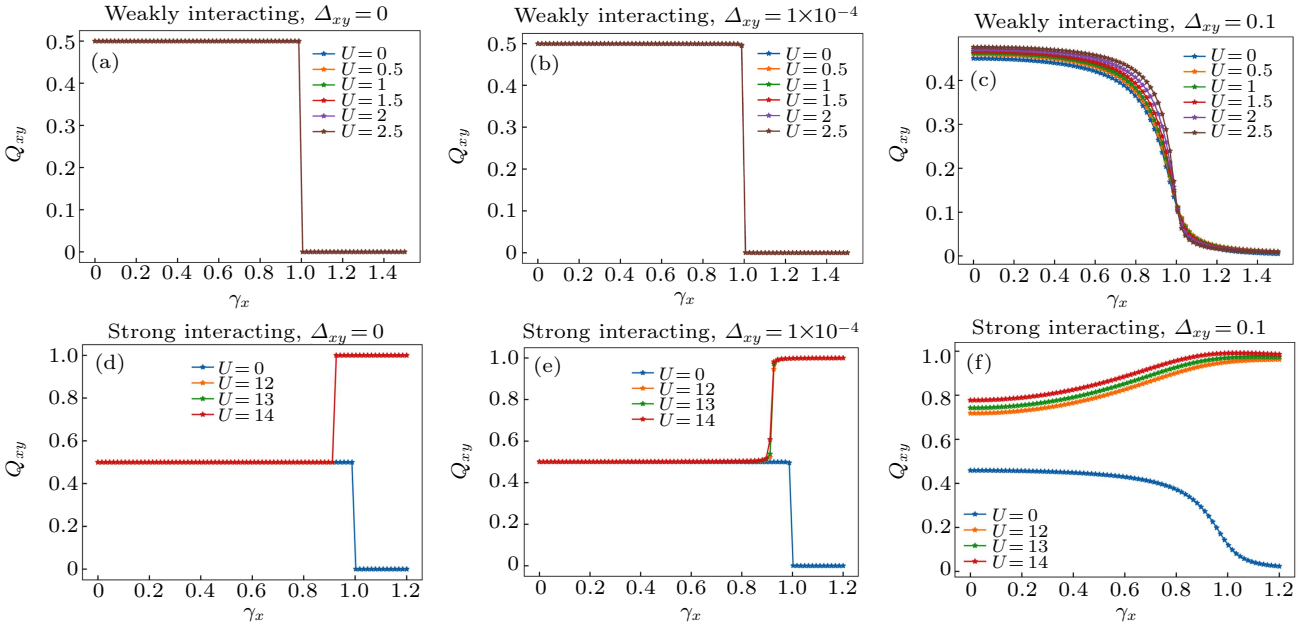


Fig. 4. The quadrupole moment Q_{xy} versus γ_x (γ_y) of the 2D BBH model for case (i) versus the staggered potential Δ_{xy} and weak interaction strength U in (a)–(c) and strong interaction strength in (d)–(f), with a lattice size of 12×12 and $\gamma_y = \gamma_x$. For the DMFT calculations, $\beta = 50$, the number of Matsubara frequencies is 256.

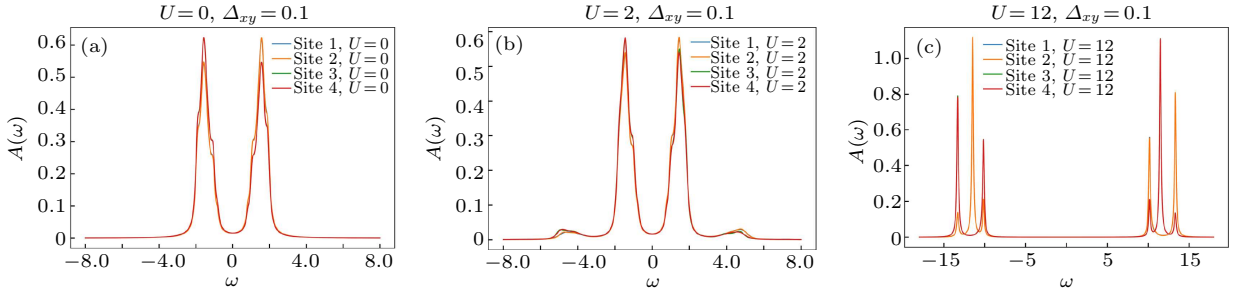


Fig. 5. Spectral functions for different interactions with $\gamma_x = \gamma_y = 0.4$. We have $\lambda_x = \lambda_y = 1$ as the energy unit with a lattice size of 12×12 and $\gamma_y = \gamma_x$. For the DMFT calculations, $\beta = 50$, the number of Matsubara frequencies is 256, and the Pade approximation[34] is adopted in the analytical continuation of Green's function to the real frequency.

We have a few words on the experimental measurement. The prediction of the multipole moments is ready to be checked by experimental measurements. Even though it is difficult to realize the BBH model in real materials, it seems promising to do this in metamaterials.[35,36] In realistic electronic systems, corner states are expected to provide boundary signatures of the underlying multipole indices. Our results for 2D systems emphasize that spatial symmetries remain the key ingredient controlling the quantization of the multipole index even in the correlated regime. This motivates using the corner charge density $n_i = -\frac{1}{\pi}\mathrm{Im}G^R_{\boldsymbol{R}_i}(\omega)|_{\omega=0}$, which can be computed straightforwardly with the R-DMFT method.

5. Conclusions

We propose a practical calculation scheme for the multipole moments in correlated materials on the level of R-DMFT. By calculations of BBH with different spatial symmetries due to staggered potentials, and different strengths of interactions we show the effectiveness of our method in exploring the properties of the multipole indices. However, its full potential is not fully unleashed. Our general method is ready to be implemented to explore a disordered correlated lattice. The close relation of polarization with the localization length,[10] and the quantum geometric tensor[32] affords us a way to explore these interesting physical quantities. Our demonstrating calculations show that the spatial symmetry is a dominant factor for the quantization of the polarization and quadrupole moments even in the correlating regime, at least in the paramagnetic phase.

Acknowledgements

T.Q. and J.H.Z. were supported by the National Natural Science Foundation of China (Grant Nos. 12174394 and U2032164). J.H.Z. was also supported by HFIPS Director's Fund (Grant Nos. YZJJQY202304 and BJPY2023B05), Anhui Provincial Major S&T Project (Grant No. s202305a12020005), and the High Magnetic Field Laboratory of Anhui Province (Grant No. AHHM-FX-2020-02). A portion of this work was supported by Chinese Academy of Sciences (Grant No. JZHKYPT-2021-08).

References

[1] Resta R 1992 *Ferroelectrics* **136** 51
[2] King-Smith R D and Vanderbilt D 1993 *Phys. Rev. B* **47** 1651
[3] Resta R 1994 *Rev. Mod. Phys.* **66** 899
[4] Ortiz G and Martin R M 1994 *Phys. Rev. B* **49** 14202
[5] Coh S and Vanderbilt D 2009 *Phys. Rev. Lett.* **102** 107603
[6] Xiao D, Chang M C and Niu Q 2010 *Rev. Mod. Phys.* **82** 1959
[7] Vaidya S, Rechtsman M C and Benalcazar W A 2024 *Phys. Rev. Lett.* **132** 116602
[8] Resta R 1998 *Phys. Rev. Lett.* **80** 1800
[9] Resta R and Sorella S 1995 *Phys. Rev. Lett.* **74** 4738
[10] Resta R and Sorella S 1999 *Phys. Rev. Lett.* **82** 370
[11] Benalcazar W A, Bernevig B A and Hughes T L 2017 *Science* **357** 61
[12] Kang B, Shiozaki K and Cho G Y 2019 *Phys. Rev. B* **100** 245134
[13] Li C A, Zhang S B, Budich J C and Trauzettel B 2022 *Phys. Rev. B* **106** L081410
[14] Xie B, Wang H X, Zhang X, Zhan P, Jiang J H, Lu M and Chen Y 2021 *Nat Rev Phys* **3** 520
[15] Yang Y B, Wang J H, Li K and Xu Y 2024 *J. Phys.: Condens. Matter* **36** 283002
[16] Zhang Y, Manjunath N, Nambiar G and Barkeshli M 2023 *Phys. Rev. X* **13** 031005
[17] Zhang Y and Barkeshli M 2025 *Phys. Rev. B* **111** 075168
[18] Benalcazar W A, Bernevig B A and Hughes T L 2017 *Phys. Rev. B* **96** 245115
[19] Georges A, Kotliar G, Krauth W and Rozenberg M J 1996 *Rev. Mod. Phys.* **68** 13
[20] Peng C, He R Q and Lu Z Y 2020 *Phys. Rev. B* **102** 045110
[21] Kang B, Lee W and Cho G Y 2021 *Phys. Rev. Lett.* **126** 016402
[22] Potthoff M 2003 *Eur. Phys. J. B* **32** 429
[23] Helmes R 2008 *Dynamical Mean Field Theory of inhomogeneous correlated systems* PhD Thesis (Koln University)
[24] Hofstetter W and Qin T 2018 *J. Phys. B: Atom. Mol. Opt. Phys.* **51** 082001
[25] Cheong S A and Henley C L 2004 *Phys. Rev. B* **69** 075111
[26] Meyer C D 2023 *Matrix Analysis and Applied Linear Algebra, Second Edition* (Philadelphia, PA: Society for Industrial and Applied Mathematics)
[27] Resta R 2021 *J. Chem. Phys.* **154** 050901
[28] Tran D T, Dauphin A, Goldman N and Gaspard P 2015 *Phys. Rev. B* **91** 085125
[29] Agarwala A and Shenoy V B 2017 *Phys. Rev. Lett.* **118** 236402
[30] Yang Y B, Qin T, Deng D L, Duan L M and Xu Y 2019 *Phys. Rev. Lett.* **123** 076401
[31] Resta R 2006 *Phys. Rev. Lett.* **96** 137601
[32] Souza I, Wilkens T and Martin R M 2000 *Phys. Rev. B* **62** 1666
[33] Mondragon-Shem I, Hughes T L, Song J and Prodan E 2014 *Phys. Rev. Lett.* **113** 046802
[34] Vidberg H J and Serene J W 1977 *J. Low Temp. Phys.* **29** 179
[35] Yatsugi K, Yoshida T, Mizoguchi T, Kuno Y, Iizuka H, Tadokoro Y and Hatsugai Y 2022 *Commun. Phys.* **5** 180
[36] Dong J, Juričić V and Roy B 2021 *Phys. Rev. Res.* **3** 023056